

# Reinforcement Learning for Laser Additive Manufacturing Scan-Order Optimisation: A Bilevel Proxy–FEA Diagnostic Framework for Reward and World-Model Diagnosis

Xian Wu<sup>a,\*</sup>, Haoran Li<sup>b</sup>, Dongbin Zhao<sup>b</sup>, Ruiyao Zhang<sup>c</sup>, Yuanqi Chu<sup>a</sup>, Bin Wang<sup>a,d</sup>

<sup>a</sup>*College of Engineering, Design and Physical Sciences, Brunel University London, Uxbridge, UB8 3PH, United Kingdom*

<sup>b</sup>*Pattern Recognition Laboratory, Institute of Automation, Chinese Academy of Sciences, Beijing, 100190, China*

<sup>c</sup>*ISIS Neutron and Muon Source, Science and Technology Facilities Council, Rutherford Appleton Laboratory, Didcot, OX11 0QX, United Kingdom*

<sup>d</sup>*Department of Mathematics, College of Engineering, Design and Physical Sciences, Brunel University London, Uxbridge, UB8 3PH, United Kingdom*

---

## Abstract

Reinforcement learning offers a promising approach for scan-order optimisation in laser additive manufacturing, where sequential scan decisions critically influence thermal accumulation, residual stress, distortion, and final part quality. A central challenge in applying RL to this domain lies in reward and world-model fidelity: full finite-element analysis is computationally prohibitive for dense in-the-loop evaluation, while cheap thermo-inspired proxy metrics, though efficient, may capture only partial aspects of the true thermo-mechanical objectives. This paper investigates a bilevel Proxy–FEA diagnostic framework for reward and world-model diagnosis in reinforcement-learning-guided scan-order optimisation. The lower level employs lightweight scan-path and thermo-inspired proxies for rapid candidate generation and preliminary policy-side screening, while the upper level utilises sparse Abaqus FEA simulations to provide simulation-based reference labels. The framework is examined on a simplified whole-track heating LDED32 stripe benchmark comprising ten representative scan strategies. Final-cooling residual Mises stress, U3 vertical distortion, and PEEQ plasticity metrics reveal an observed stress–distortion trade-off rather than a single monotonic quality objective. Within the evaluated set, the center\_out strategy emerges as a robust compromise candidate, while

---

\*Corresponding author.

*Email address:* Bin.Wang@brunel.ac.uk (Bin Wang)

raster\_left\_to\_right and edge\_in form opposing endpoints of the trade-off. Proxy-FEA alignment analysis shows that current cheap path-based metrics predominantly capture distortion-related (U3) behaviour and exhibit only weak correlation with the sparse FEA reference labels. These findings highlight that proxy-only reward designs risk misalignment in future RL training and underscore the value of sparse FEA reference signals for diagnostic-guided reward and world-model refinement prior to large-scale policy optimisation.

*Keywords:* Reinforcement learning, laser additive manufacturing, scan-order optimisation, finite-element analysis, reward modelling, world-model diagnosis, residual stress, distortion, LDED

---

## 1. Introduction

Laser additive manufacturing (LAM), including laser powder bed fusion (LPBF) and laser directed energy deposition (LDED), enables the fabrication of geometrically complex metallic components through localised, layer-wise energy input. However, the same concentrated heat source also produces steep thermal gradients, repeated heating and cooling cycles, and path-dependent thermal accumulation. These thermal histories strongly influence microstructure, residual stress, distortion, cracking susceptibility, and final part quality. Among the process variables governing these effects, scan strategy has been widely recognised as a critical factor because it determines the spatial and temporal sequence of heat input. Different scan patterns, such as raster, stripe, island, chessboard, interlaced, rotated, and multi-laser strategies, have been shown to alter temperature evolution, residual stress development, and deformation behaviour in laser-based metal AM [1, 2, 3]. Scan-order design is therefore treated here as part of process-quality control rather than as a purely geometric path-planning choice.

Residual stress and distortion are particularly important outcomes because they directly affect dimensional accuracy, structural integrity, and post-processing requirements in metal AM. Both arise from non-uniform heating, constrained thermal expansion and contraction, and cyclic reheating during layer-wise fabrication. They are therefore coupled thermo-mechanical consequences of the same process history. However, they are not interchangeable quality indicators. A scan strategy that reduces one residual response may not necessarily minimise another, especially when thermal gradients, boundary con-

straints, local plasticity, and global displacement modes respond differently to the heat-input sequence. Reviews of distortion and residual stress in AM have emphasised their coupled formation mechanisms and the role of process parameters and scan strategy in their mitigation [4, 5]. This motivates scan-strategy evaluation as a multi-metric problem rather than a single-objective search for thermal uniformity or residual-stress reduction alone.

Computational modelling and data-driven methods have been increasingly used to analyse and optimise process–quality relationships in metal AM. Thermo-mechanical finite-element analysis (FEA) can provide physically informative predictions of temperature history, residual stress, and distortion, but it is computationally expensive when many candidate scan sequences or process settings must be evaluated. Machine learning and surrogate modelling have therefore been explored for process–structure–property modelling, process-parameter optimisation, residual-stress prediction, distortion mitigation, and simulation acceleration in LPBF and related laser AM processes [6, 7, 8]. Simulation-guided process design has also been used in DED to reduce iterative simulation burden when optimising laser power or melt-pool behaviour [9]. These studies demonstrate the value of combining physics-based simulation and data-driven acceleration, but most remain prediction-, parameter-, or process-control-oriented rather than focused on the reward/evaluator fidelity required for sequential scan-order learning.

Reinforcement learning (RL) is attractive for scan-order optimisation because the problem is naturally sequential: each action changes the remaining unprocessed region and affects delayed thermal and mechanical outcomes. RL has already been explored for AM process control, including melt-pool or thermal regulation, process-parameter adjustment, and stability-aware control [10, 11, 12]. More recently, RL-based scan-path or toolpath generation has begun to appear in LPBF, with agents trained using temperature-field information, thermal-uniformity rewards, or fast thermal surrogate predictions [13, 14, 15]. These studies show the feasibility of RL-based process or scan-path control, but they also make reward and evaluation-environment design central. A central remaining issue is not simply whether RL can generate scan paths, but whether the reward or task-level world-model signal used during learning preserves the residual stress–distortion preference structure relevant to final part quality.

To address this gap, this study investigates a bilevel Proxy–FEA diagnostic approach for RL-guided scan-order optimisation in laser additive manufacturing. The lower level uses cheap scan-path and thermo-inspired proxy metrics for fast candidate evaluation and preliminary screening. The upper level applies sparse Abaqus FEA reference evaluation to selected complete scan strategies, producing simulation-based residual outcome labels from final-cooling fields. The relationship between the two levels is then analysed through Proxy–FEA alignment. This alignment is not intended to validate the proxy as a surrogate replacement for FEA. Instead, it is used diagnostically to identify which physical trends the proxy captures, where it fails, and how future RL reward or task-level world-model design should be revised. The approach is instantiated on a simplified LDED32 benchmark consisting of 32 discrete scan tracks under a whole-track heating abstraction. Ten completed scan strategies are evaluated using residual Mises stress, vertical U3 distortion range, and a PEEQ-based plasticity indicator.

The study contributes a reward/world-model diagnosis workflow for future RL-guided scan-order optimisation by framing scan-order selection as an RL-oriented evaluation problem in which reward fidelity is treated as a first-order concern. It couples fast lower-level proxy screening with sparse upper-level FEA reference evaluation and uses the resulting Proxy–FEA alignment to examine whether cheap proxy metrics preserve the residual stress–distortion preference structure of the FEA reference labels. Within the simplified LDED32 benchmark, the results show that scan-order performance is better interpreted as a stress–distortion trade-off than as a single monotonic optimisation objective, while the current proxy metrics capture selected trends but do not robustly recover the sparse FEA reference labels. These findings point to the need for FEA-guided reward and world-model refinement before large-scale policy training. The scope of the present work is intentionally bounded: it does not claim final RL policy success, experimental validation, calibrated LDED physics, or a validated FEA-replacing surrogate. Instead, it positions the current benchmark as a diagnostic closure study that prepares the ground for higher-entropy RL policy-learning benchmarks.

## **2. A Bilevel Proxy–FEA Diagnostic Framework for RL-Guided Scan-Order Optimisation**

Reinforcement-learning-guided scan-order optimisation requires an evaluation signal that is both computationally efficient and physically meaningful. In laser additive manufactur-

ing, this requirement is difficult to satisfy because the thermo-mechanical consequences of a scan sequence are path-dependent, delayed, and multi-metric. Full finite-element analysis (FEA) can provide richer simulation-based information about residual stress and distortion, but it is not practical as a dense online reward source during reinforcement learning. Conversely, cheap scan-path or thermo-inspired proxy metrics can be evaluated rapidly, but may only capture partial aspects of the final thermo-mechanical response. This separation between inexpensive approximate evaluation and sparse high-cost reference evaluation is conceptually related to multifidelity modelling, where low-fidelity models are used to reduce evaluation cost while high-fidelity models remain available for correction, inference, or optimisation support [16].

In this exploratory study, we investigate a bilevel Proxy–FEA diagnostic approach. The lower level uses cheap proxy descriptors for fast candidate generation and preliminary screening. The upper level uses sparse FEA reference evaluations to provide simulation-based residual outcome labels. The relationship between these two levels is analysed through Proxy–FEA alignment, with the objective of diagnosing reward and world-model mismatch before large-scale RL policy training is attempted. Accordingly, the present work is positioned as a diagnostic study rather than as a claim of completed policy learning, proxy replacement of FEA, calibrated LDED physics, or validated surrogate modelling.

In model-based reinforcement learning, learned or approximate models are often used to support planning and policy learning, as in Dyna-style architectures and neural world-model approaches [17, 18]. Here, the term world model is used in a task-level sense. It refers to the evaluation structure that maps candidate scan-order decisions to approximate process-quality indicators. It does not denote a trained latent-dynamics neural model. The present approach therefore focuses on reward and world-model diagnosis rather than claiming a completed policy-learning loop.

### *2.1. RL-oriented scan-order formulation*

Let the build domain be decomposed into a finite set of scannable units,

$$\mathcal{G} = \{g_i\}_{i=1}^N,$$

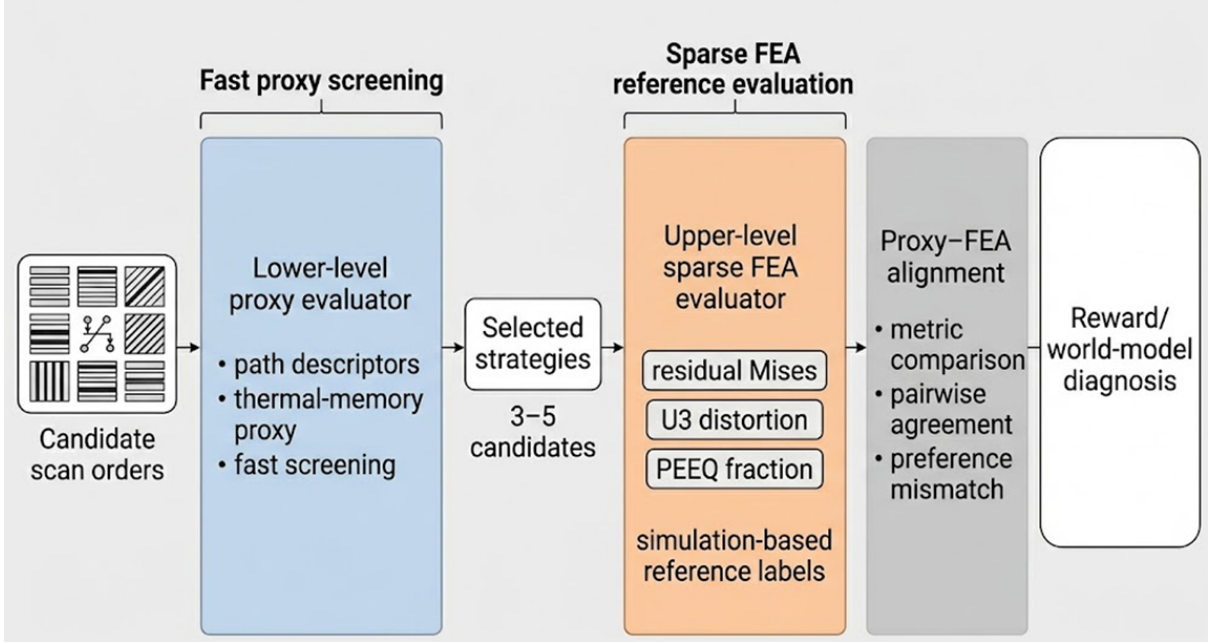


Figure 1: Bilevel Proxy- $\text{FEA}$  diagnostic framework for RL-guided scan-order optimisation. The lower level uses cheap scan-path and thermo-inspired proxy descriptors for fast candidate screening, while the upper level applies sparse FEA reference evaluation to selected complete scan strategies. Proxy- $\text{FEA}$  alignment compares proxy-induced and FEA-induced preferences to diagnose reward/world-model mismatch before future large-scale policy learning. The framework is diagnostic and does not imply proxy replacement of FEA or completed RL policy learning.

where each  $g_i$  denotes a track, stripe, or local scan region. A scan-order trajectory is represented as a permutation over  $\mathcal{G}$ ,

$$\tau = (a_1, a_2, \dots, a_N), \quad a_t \in \mathcal{G}, \quad a_i \neq a_j \quad \forall i \neq j. \quad (1)$$

This permutation structure makes scan-order optimisation naturally compatible with an RL formulation: at each decision step, an agent or planner selects the next unprocessed scan unit, while the eventual reward should reflect the quality of the completed build. However, the most relevant quality indicators, such as residual stress and distortion, are not available as immediate stepwise feedback. They emerge from the complete thermal-mechanical history of the scan sequence.

The key issue addressed in this section is therefore not the choice of a particular RL optimiser, but the reliability of the evaluation signal that would guide future policy optimisation. This emphasis is motivated by the broader RL concern that misspecified rewards can induce agents to optimise behaviours that differ from the designer’s intended objective [19]. The present study does not claim that PPO or an equivalent RL algorithm has converged to an optimal scan strategy. Instead, it formalises the diagnostic evaluation

layer required before such policy learning can be pursued responsibly.

### 2.2. Lower-level proxy evaluator

The lower-level proxy evaluator maps a scan-order trajectory to a vector of inexpensive sequence descriptors,

$$\mathbf{p}(\tau) = \Phi_{\text{proxy}}(\tau) = [p_1(\tau), p_2(\tau), \dots, p_K(\tau)]^\top \in \mathbb{R}^K. \quad (2)$$

The components of  $\mathbf{p}(\tau)$  may include path-spacing, jump-distance, neighbour-gap, clustering, boundary exposure, symmetry, and simplified thermal-memory indicators. These descriptors are designed to capture scan-order features that are computationally cheap and potentially relevant to heat accumulation or distortion risk.

A generic scalar proxy score can be written as

$$J_{\text{proxy}}(\tau; \boldsymbol{\alpha}) = \boldsymbol{\alpha}^\top \tilde{\mathbf{p}}(\tau) = \sum_{k=1}^K \alpha_k \tilde{p}_k(\tau), \quad (3)$$

where  $\tilde{\mathbf{p}}(\tau)$  denotes the normalised proxy descriptor vector and  $\boldsymbol{\alpha}$  denotes proxy weighting coefficients.

The proxy score is useful because it can be evaluated rapidly over many candidate scan orders. In future RL-oriented workflows, such a score could support policy-side screening, candidate generation, or approximate reward shaping. In the current simplified setting, however,  $J_{\text{proxy}}$  is not treated as a validated surrogate for thermo-mechanical response. It is treated as a candidate evaluation signal whose agreement with FEA reference outcomes must be diagnosed.

### 2.3. Sparse FEA reference evaluator

The upper-level evaluator maps selected complete scan sequences to simulation-based residual outcome labels,

$$\mathbf{y}_{\text{FEA}}(\tau_i) = \Psi_{\text{FEA}}(\tau_i) = [y_\sigma(\tau_i), y_u(\tau_i), y_p(\tau_i)]^\top, \quad (4)$$

where  $y_\sigma$  is a residual Mises stress metric,  $y_u$  is a vertical distortion metric, and  $y_p$  is a plasticity-related metric. In the current LDED32 implementation, these correspond to final-cooling residual Mises stress, U3 distortion range, and PEEQ-based plastic fraction. In the present implementation, these quantities are extracted from final-cooling residual fields and used as Proxy–FEA alignment analysis.

A composite FEA reference score is defined as

$$J_{\text{FEA}}(\tau_i; \boldsymbol{\beta}) = \boldsymbol{\beta}^\top \tilde{\mathbf{y}}_{\text{FEA}}(\tau_i) = \beta_\sigma \tilde{y}_\sigma(\tau_i) + \beta_u \tilde{y}_u(\tau_i) + \beta_p \tilde{y}_p(\tau_i), \quad (5)$$

with

$$\beta_j \geq 0, \quad \sum_j \beta_j = 1.$$

Here,  $\tilde{\mathbf{y}}_{\text{FEA}}$  denotes normalised reference labels. Lower values of  $J_{\text{FEA}}$  indicate more favourable performance under the selected composite objective.

The FEA reference evaluator is sparse by design. It is applied only to selected complete scan strategies, rather than to every intermediate RL action. This reflects the practical computational constraint that full thermo-mechanical FEA cannot serve as a dense online reward source. The role of FEA in the present approach is therefore diagnostic and corrective: it provides Proxy-FEA alignment analysis against which cheap proxy preferences can be audited.

These FEA labels should not be interpreted as experimental ground truth or as evidence of a calibrated high-fidelity LDED model. They are reference outcomes within the current simplified simulation setting, and all benchmark-level interpretations are therefore restricted to this simulation-based diagnostic setting.

#### 2.4. Proxy-FEA alignment for reward and world-model diagnosis

The central diagnostic question is whether the preference structure induced by the cheap proxy evaluator is consistent with the preference structure induced by the sparse FEA reference evaluator. Given a small exploratory set of  $M$  evaluated strategies,

$$\mathcal{D}_{\text{FEA}} = \{(\tau_i, \mathbf{y}_{\text{FEA}}(\tau_i), J_{\text{FEA}}(\tau_i))\}_{i=1}^M,$$

Proxy-FEA alignment compares  $J_{\text{proxy}}$ , individual FEA metrics, and the composite FEA reference score.

A useful diagnostic is pairwise ranking disagreement, following the preference-consistency logic commonly used in learning-to-rank and pairwise comparison settings [20]. For any two strategies  $\tau_i$  and  $\tau_j$ , a proxy-induced preference is inconsistent with the FEA-induced preference if the two scores order the pair differently. The pairwise mismatch rate can be

written as

$$\mathcal{L}_{\text{pair}} = \frac{2}{M(M-1)} \sum_{1 \leq i < j \leq M} \mathbb{I}[\text{sgn}(J_{\text{proxy}}(\tau_i) - J_{\text{proxy}}(\tau_j)) \neq \text{sgn}(J_{\text{FEA}}(\tau_i) - J_{\text{FEA}}(\tau_j))], \quad (6)$$

where  $\mathbb{I}[\cdot]$  is the indicator function. The corresponding pairwise agreement rate is

$$A_{\text{pair}} = 1 - \mathcal{L}_{\text{pair}}. \quad (7)$$

This pairwise view is useful for RL-guided scan-order optimisation because a future policy does not necessarily require exact regression of the FEA score, but it does require a reward signal that preserves enough preference structure to avoid systematically favouring inferior scan strategies. If the proxy and FEA reference disagree on many pairwise comparisons, proxy-only reward design may bias the learning process toward an incomplete or misaligned objective.

In the present work, Proxy–FEA alignment is used qualitatively and diagnostically. It is not used to calibrate final reward weights, validate a surrogate model, or claim that the cheap proxy can replace FEA. Therefore, proxy metrics are interpreted as diagnostic indicators rather than validated predictors of the composite FEA response.

### *2.5. Multi-metric preference interpretation*

The FEA reference labels contain multiple residual outcome metrics. Scan-order optimisation is therefore treated as a multi-metric preference problem rather than a single scalar thermal-uniformity problem. This interpretation is consistent with multi-objective optimisation, where candidate solutions are compared relative to trade-offs among competing objectives rather than a single universal optimum [21]. In simplified notation,

$$\min_{\tau} \mathbf{Y}(\tau) = [y_{\sigma}(\tau), y_u(\tau), y_p(\tau)]^{\top}. \quad (8)$$

A strategy is preferable only relative to the selected trade-off between stress, distortion, and plasticity-related indicators. For example, a scan order may reduce the residual Mises stress metric while increasing the U3 distortion metric, or vice versa. In such cases, a scalar proxy reward based on a single path descriptor may fail to represent the relevant preference structure.

For the current simplified LDED32 setting, this multi-metric interpretation is used to interpret FEA-ranked strategy behaviour and to motivate Proxy–FEA alignment. It is

not used to claim a universal Pareto-optimal scan strategy outside the evaluated strategy set.

### 2.6. Diagnostic workflow

The diagnostic workflow used in this study can be summarised as

$$\boxed{\Pi(\mathcal{G}) \xrightarrow{\Phi_{\text{proxy}}} \mathbf{p}(\tau) \xrightarrow{\text{screening}} \{\tau_i\}_{i=1}^M \xrightarrow{\Psi_{\text{FEA}}} \mathbf{y}_{\text{FEA}}(\tau_i) \xrightarrow{\text{Proxy-FEA alignment}} \Delta_{\text{reward/world-model}}} \quad (9)$$

where  $\Delta_{\text{reward/world-model}}$  denotes the diagnosed mismatch between cheap proxy preferences and sparse FEA reference preferences.

This workflow is intended to support RL-guided scan-order optimisation by improving the reliability of the evaluation signal before policy training. It does not require FEA to be called at every RL step, and it does not assume that cheap proxies are physically authoritative. Instead, sparse FEA reference evaluation is used as a diagnostic correction layer for future reward and world-model refinement.

For the current study, this diagnostic workflow is instantiated on a simplified LDED32 scan-order benchmark with ten evaluated strategies. The following section describes the benchmark, the scan strategy set, and the FEA reference labelling procedure.

## 3. LDED32 Benchmark and FEA Reference Labelling

### 3.1. Simplified LDED32 scan-order benchmark

The diagnostic approach was instantiated on a simplified LDED32 scan-order benchmark. The benchmark represents a laser directed energy deposition (LDED)-style stripe configuration in which the build region is divided into 32 discrete scan tracks. Each scan strategy is defined by the order in which these tracks are processed. The benchmark is used here as a controlled setting for examining scan-order-dependent residual outcomes and Proxy-FEA alignment. Such a track-order abstraction is motivated by the established sensitivity of thermal and residual responses to scan strategy in laser-based metal additive manufacturing [1, 2, 3].

A whole-track heating abstraction was used. Under this abstraction, each selected track is activated as a complete scan unit according to the prescribed order, rather than being represented by a fully resolved moving heat source. This simplification makes the benchmark computationally tractable and keeps the analysis focused on track-order effects. The

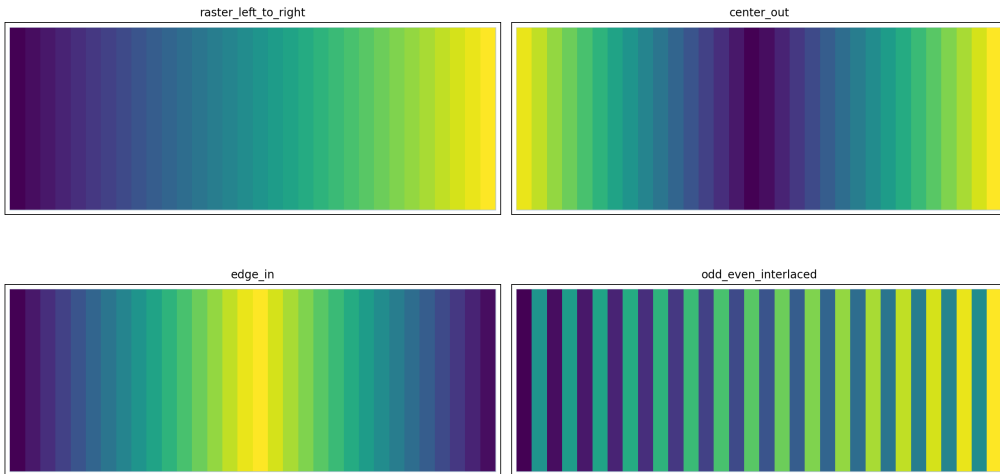


Figure 2: Simplified LDED32 scan-order benchmark. The build region is divided into 32 discrete scan tracks, each treated as a complete scan unit under the whole-track heating abstraction. The labelled track IDs define the scan-order permutation used in the evaluated strategies. The benchmark is used as a controlled simulation setting for reward and world-model diagnosis rather than as a calibrated high-fidelity LDED model.

abstraction differs from fully resolved moving heat-source or element-activation thermal models commonly used in welding and additive manufacturing process simulation [22, 23]. The resulting model should therefore be interpreted as a controlled simulation setting for reward and world-model diagnosis, not as a calibrated high-fidelity representation of LDED physics.

The 32-track layout provides a compact but interpretable scan-order space. It is sufficiently structured to produce different residual stress and distortion responses across scan strategies, while remaining small enough for sparse FEA reference evaluation. However, the benchmark is not used as evidence of final RL policy learning. Its role in this paper is to examine whether cheap scan-order proxy metrics align with higher-cost FEA reference outcomes in a controlled setting.

The labelled LDED32 geometry is shown in Fig. 2. The labelled track-ID version is used in the methods section because it directly supports the scan-order description and defines the permutation space used by the evaluated strategies.

### 3.2. Evaluated scan strategy set

In this exploratory study, a fixed set of ten completed scan strategies was evaluated. The strategy set covers baseline, symmetric, interlaced, distance-aware, proxy-informed, and

Table 1: Evaluated scan strategies in the LDED32 benchmark. The table lists the strategy identifier, scan-order design principle, and role in the diagnostic analysis.

Strategy identifier	Design principle	Diagnostic role
<code>raster_left_to_right</code>	Sequential left-to-right raster order	Baseline; low-Mises/high-U3 endpoint
<code>odd_even_interlaced</code>	Odd-even interlaced track ordering	Interlaced baseline
<code>center_out</code>	Tracks processed from centre toward edges	Robust compromise candidate
<code>edge_in</code>	Tracks processed from edges toward centre	Low-U3/high-Mises endpoint
<code>greedy_maximin</code>	Distance-aware greedy ordering	Spatial separation baseline
<code>smartscan_proxy</code>	Proxy-variance-guided ordering	Proxy-informed candidate
<code>multilag_jump</code>	Regular multi-lag jump ordering	Regular jump-pattern candidate
<code>block_quarters</code>	Block-interleaved quarter ordering	Blockwise interleaving candidate
<code>windowed_disp.</code>	Windowed maximum-dispersion ordering	Local dispersion candidate
<code>center_edge</code>	Alternating centre-edge ordering	Mixed centre/edge candidate

mixed scan-order behaviours. The evaluated set includes raster-like scanning, centre-out scanning, edge-in scanning, odd-even interlacing, greedy distance-based ordering, proxy-variance-guided ordering, multi-lag regular jumps, block-interleaved ordering, windowed dispersion, and centre-edge alternating ordering.

These strategies are not treated as an exhaustive optimisation set. Instead, they provide a controlled reference set for diagnosing stress–distortion behaviour and Proxy–FEA alignment. This is important because the objective of the current work is not to claim that a trained RL agent discovered the best scan order, but to identify whether the available proxy metrics provide reliable preference information for future RL reward design.

The evaluated strategies are summarised in Table 1, including their identifiers, scan-order design principles, and roles in the present diagnostic analysis.

### 3.3. Sparse Abaqus FEA reference workflow

For each selected scan strategy, an Abaqus FEA reference simulation was used to obtain residual outcome labels. Thermo-mechanical FEA has been widely used to estimate residual stress and distortion in laser-assisted and directed-energy-deposition additive manufacturing processes [24, 25, 7]. In the present workflow, the FEA reference layer was applied sparsely to complete scan-order trajectories rather than densely at each intermediate scan decision. This is consistent with the intended role of FEA in the diagnostic approach: FEA provides higher-cost simulation-based reference information

for selected complete strategies, while the lower-level proxy remains responsible for fast candidate generation and screening.

The FEA workflow consisted of completed scan-strategy simulations, final-cooling residual metric extraction, final-step consistency checks, ranking robustness analysis, representative field-map extraction, and Proxy–FEA alignment outputs. These steps provide the simulation-derived reference-label chain used in the present manuscript.

The FEA reference outputs are simulation-based labels. They are used to compare scan strategies within the current simplified LDED32 setting. They are not presented as experimental measurements, nor as evidence of a calibrated high-fidelity LDED model. This scope limitation is retained throughout the Methods, Results, and Discussion sections.

#### *3.4. Final-cooling residual metric extraction*

The FEA reference labels were extracted from the final-cooling last frame. Residual stress and distortion are commonly treated as key thermo-mechanical quality indicators in metal additive manufacturing [4, 5]. Three residual outcome metrics were used:

$$\mathbf{y}_{\text{FEA}}(\tau_i) = [y_\sigma(\tau_i), y_u(\tau_i), y_p(\tau_i)]^\top,$$

where  $y_\sigma$  denotes the residual Mises stress metric,  $y_u$  denotes the U3 vertical distortion metric, and  $y_p$  denotes the PEEQ-based plasticity metric.

The residual Mises metric was computed over the scan region after excluding boundary-condition-dominated regions. In the current implementation, the main stress metric is represented by a high-stress summary statistic, specifically the scan-region residual Mises top-five mean after boundary-condition exclusion. This avoids relying only on a single extreme nodal value while still capturing high residual stress concentration.

The U3 metric was computed as the vertical displacement range over the scan region, again excluding boundary-condition-dominated regions. This metric is used as the primary distortion indicator. The U3 range is particularly important because the current results show that strategies with favourable residual stress behaviour may still produce unfavourable vertical distortion.

The PEEQ metric was represented as a plastic-fraction indicator over the scan region. In the current dataset, this metric has limited discriminative value under the selected

threshold and strategy set. It is therefore retained as part of the reference label vector and composite score, but it should not be overinterpreted as the dominant physical discriminator.

The three extracted metrics can be formally expressed as follows:

$$\mathbf{y}_{\text{FEA}}(\tau_i) = \begin{cases} y_\sigma(\tau_i) & = \text{Mises}_{\text{top5,scan region excluding BC}}, \\ y_u(\tau_i) & = \max_{\Omega_s} U3 - \min_{\Omega_s} U3, \\ y_p(\tau_i) & = \text{frac}(\text{PEEQ} > \epsilon_p)_{\Omega_s}, \end{cases}$$

where  $\Omega_s$  denotes the scan-region evaluation domain after boundary-condition exclusion, and  $\epsilon_p$  denotes the PEEQ threshold used for the plastic-fraction calculation. where  $\tilde{y}_\sigma$ ,  $\tilde{y}_u$ , and  $\tilde{y}_p$  denote normalised residual Mises, U3 distortion, and PEEQ plastic-fraction metrics, respectively. Lower values of  $J_{\text{FEA}}$  indicate more favourable performance under the selected composite reference objective.

The composite score was used to generate the baseline FEA reference ranking. Alternative weighting schemes were then used to examine ranking robustness under different stress-, distortion-, and plasticity-emphasis assumptions. This robustness check is important because the scan-order problem is inherently multi-metric. A strategy that performs well under a stress-weighted objective may not be preferred under a distortion-weighted objective.

The ranking analysis is used as a diagnostic reference for later Proxy–FEA alignment. It is not treated as a calibrated universal objective function. The weights are not claimed to be physically optimal or experimentally calibrated. Their role is to expose the preference structure of the evaluated strategy set and to test whether the main interpretation remains stable under plausible metric-weight variations.

In the manuscript, the compact FEA ranking table is presented as Table 2. The raw full reference label table is better placed in the Supplementary Information because it is too wide for the main text.

### 3.5. Benchmark scope

All conclusions from this section are limited to the current simulation-based, simplified whole-track heating LDED32 stripe benchmark with ten evaluated scan strategies. The

Table 2: FEA reference ranking of the ten evaluated scan strategies. Lower composite score indicates more favourable performance under the selected reference objective.

Rank	Strategy	Mises top-5 (MPa)	U3 range (mm)	PEEQ frac. (%)	Score
1	<code>center_out</code>	203.481	0.452	99.997	0.266
2	<code>odd_even</code>	239.073	0.897	99.405	0.380
3	<code>block_quarters</code>	301.565	0.490	99.406	0.405
4	<code>greedy_maximin</code>	252.768	0.824	99.607	0.416
5	<code>multilag_jump</code>	337.045	0.491	99.059	0.434
6	<code>center_edge</code>	371.445	0.554	98.482	0.447
7	<code>edge_in</code>	407.721	0.276	98.558	0.460
8	<code>raster</code>	194.164	1.607	99.361	0.466
9	<code>windowed_disp.</code>	307.889	0.507	99.912	0.489
10	<code>smartscan_proxy</code>	353.251	0.527	99.268	0.505

benchmark is used here to support reward and world-model diagnosis for RL-guided scan-order optimisation, not to provide final experimental validation of LDED physics or final proof of RL policy performance.

The compact LDED32 setting provides a controlled environment in which stress–distortion trade-offs and proxy mismatch can be examined. At the same time, its strategy space is too low-entropy for strong claims about policy generalisation. Future RL policy-learning work should therefore move toward a higher-entropy benchmark while retaining sparse FEA reference evaluation as a correction and diagnostic layer.

## 4. Results

### 4.1. FEA reference ranking and metric decomposition

The simulation-based FEA reference ranking of the ten evaluated scan strategies is summarised in Table 2 and Fig. 3. Table 2 reports the compact numerical ranking based on the final-cooling residual metrics, while Fig. 3 decomposes the normalised metric contributions to the composite FEA reference score. This combined table–figure presentation allows the ranking to be interpreted in terms of its underlying residual stress, distortion, and plasticity-related components.

Within the current simplified LDED32 benchmark, `center_out` emerges as a robust compromise candidate among the ten evaluated strategies. Its performance is best interpreted as a balanced response across the main residual metrics rather than as an absolute minimum in every individual metric. This distinction is important because the evaluated scan strategies do not follow a single monotonic quality trend. Instead, the ranking reflects a trade-off between residual Mises stress, U3 vertical distortion, and the less discriminative PEEQ plastic-fraction term.

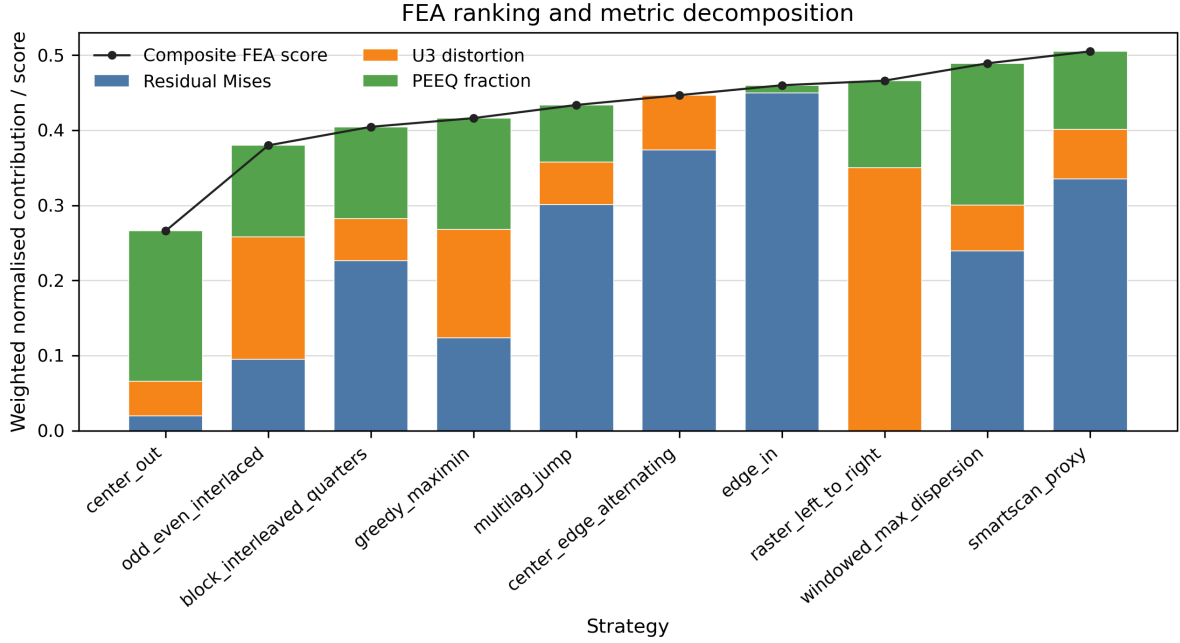


Figure 3: FEA reference ranking and normalised metric decomposition. The figure shows the sparse FEA teacher signals of the ten evaluated scan strategies, together with the normalised contributions from residual Mises stress, U3 distortion, and PEEQ plastic fraction.

The metric decomposition in Fig. 3 shows that `raster_left_to_right` and `edge_in` occupy different metric regimes. `raster_left_to_right` exhibits favourable residual Mises behaviour but unfavourable U3 distortion, whereas `edge_in` exhibits comparatively favourable U3 behaviour but higher residual Mises stress. These strategies therefore serve as stress–distortion endpoints within the evaluated strategy set, not as generally good or bad scan strategies.

The PEEQ plastic-fraction metric provides limited separation under the current threshold. It is retained in the composite score for completeness, but the main ranking interpretation is driven primarily by residual Mises stress and U3 distortion. This should not be interpreted as evidence that plasticity is physically unimportant; it only indicates limited discrimination in the current labelled set.

#### 4.2. Stress–distortion trade-off

The FEA reference labels show an observed stress–distortion trade-off among the ten evaluated strategies in the current benchmark. Figure 4 plots the residual Mises metric against the U3 distortion range. The strategies do not collapse onto a single quality axis: reducing one residual outcome can coincide with an increase in another.

The trade-off structure is particularly visible in the relative positions of `raster_left_to_right`,

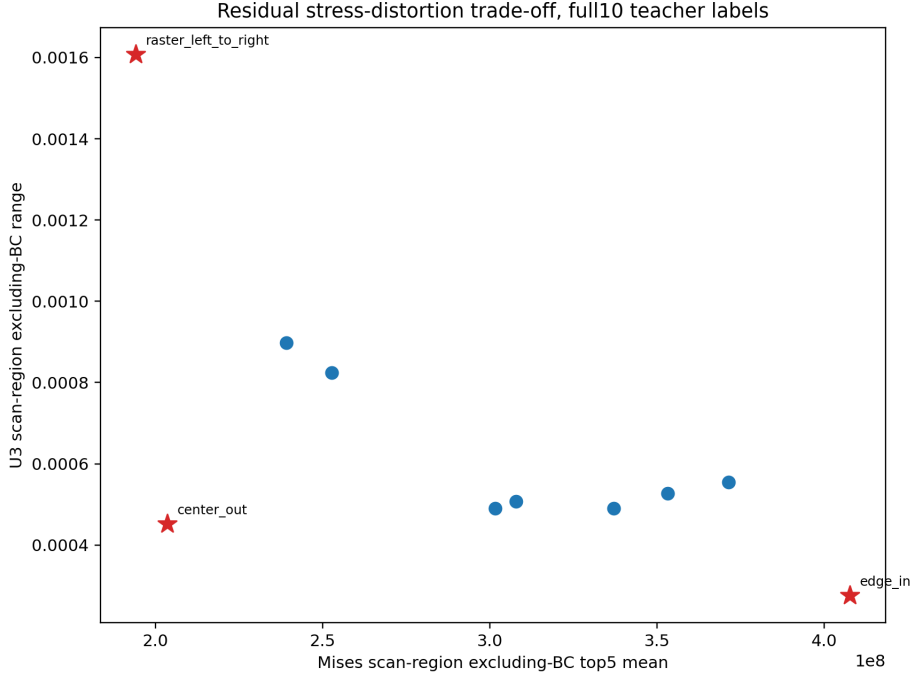


Figure 4: Stress–distortion trade-off in the LDED32 benchmark. Residual Mises stress is plotted against U3 vertical distortion range for the ten evaluated scan strategies. `raster_left_to_right`, `center_out`, and `edge_in` illustrate the low-Mises/high-U3 endpoint, compromise region, and low-U3/high-Mises endpoint, respectively.

`center_out`, and `edge_in`. `raster_left_to_right` lies toward the low-Mises/high-U3 side of the objective space, while `edge_in` lies toward the low-U3/high-Mises side. `center_out` occupies an intermediate region and is therefore better interpreted as a robust compromise candidate than as a universal optimum.

This trade-off highlights the importance of multi-metric reward design for future RL-guided scan-order optimisation. A reward signal based only on path spacing, local reheating avoidance, residual stress reduction, or distortion reduction may favour a strategy near one endpoint while neglecting another residual outcome. The FEA reference scatter suggests that scan-order optimisation in this simplified benchmark should be treated as a multi-metric preference problem, consistent with the broader multi-objective optimisation view in which candidate solutions are interpreted through trade-offs rather than a single universal optimum [21].

The ranking robustness analysis in Fig. 6 further supports this interpretation. When the metric weighting shifts toward stress or distortion, the ranking changes accordingly. This indicates that the observed strategy ordering is not only a consequence of the baseline composite weighting, but reflects competing residual stress and distortion preferences in

the evaluated set.

#### *4.3. Residual field-map evidence for compromise and endpoint strategies*

Figure 5 compares representative final-cooling residual field maps for `raster_left_to_right`, `center_out`, and `edge_in`. These three strategies were selected because they represent the main behaviours observed in the FEA reference space: a low-Mises/high-U3 endpoint, a compromise candidate, and a low-U3/high-Mises endpoint. The figure focuses on Mises and U3 maps because these are the dominant discriminating metrics in the current dataset.

The field maps provide spatial support for the ranking interpretation. The `raster_left_to_right` case shows why a low-Mises ranking alone is insufficient: despite favourable residual Mises behaviour, its U3 map indicates a larger vertical distortion response. Conversely, the `edge_in` case shows that a distortion-favourable strategy may carry a residual-stress penalty. `center_out` avoids the more extreme behaviour of both endpoint strategies, further supporting its interpretation as a robust compromise candidate among the evaluated set.

The field-map evidence also helps prevent overinterpretation of the composite score. The ranking table identifies the ordering, while the field maps show how different residual modes are spatially distributed. This is especially important for manufacturing interpretation, where local residual concentration and global distortion may have different process consequences. Similar thermo-mechanical AM simulation studies and residual-stress reviews have also emphasised the need to interpret residual stress and distortion through their spatial distributions rather than through scalar indicators alone [25, 7].

PEEQ and thermal-state maps are treated as supplementary diagnostic evidence. PEEQ is weakly discriminative under the current threshold, while NT11 thermal-state maps provide useful audit context but are not central to the main stress–distortion claim.

#### *4.4. Ranking robustness across metric weightings*

Figure 6 summarises the robustness of the FEA reference ranking under alternative metric-weighting schemes. The purpose of this analysis is not to calibrate a universal physical objective, but to examine whether the main interpretation remains stable when residual stress, distortion, or plasticity terms are emphasised differently.

Representative final-cooling residual field maps

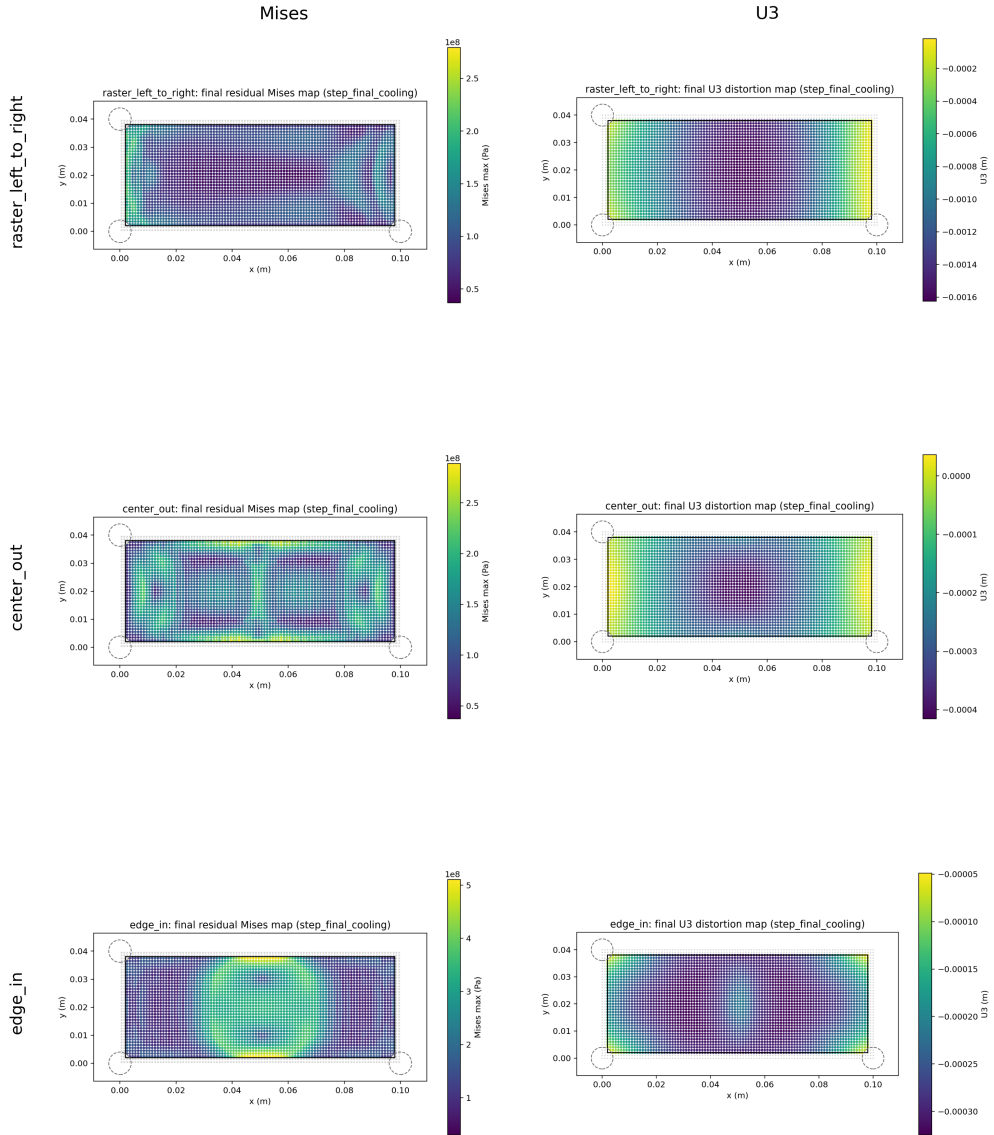


Figure 5: Representative final-cooling residual field maps. Mises and U3 maps are shown for raster\_left\_to\_right, center\_out, and edge\_in. The selected strategies illustrate the low-Mises/high-U3 endpoint, the compromise candidate, and the low-U3/high-Mises endpoint in the current LDED32 benchmark.

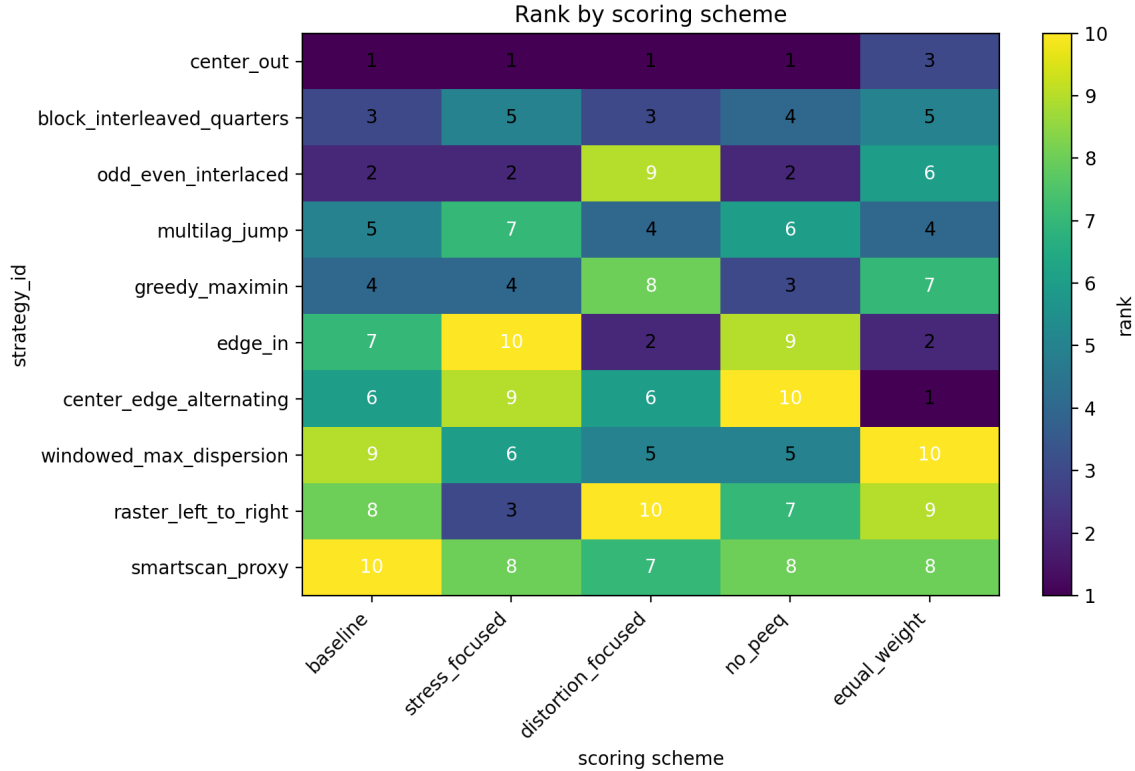


Figure 6: Ranking robustness across metric-weighting schemes. The heatmap summarises how scan-strategy ranking changes under different stress-, distortion-, and plasticity-emphasis assumptions. The analysis supports the interpretation of `center_out` as a robust compromise candidate while showing that ranking changes when stress or distortion is emphasised.

The robustness results support the interpretation of `center_out` as a compromise candidate. Its value is not that it dominates every metric under every weighting, but that it remains competitive across the evaluated weighting schemes and avoids the more extreme behaviour associated with `raster_left_to_right` and `edge_in`. This is why `center_out` is described as a robust compromise candidate rather than an optimal scan strategy.

The robustness analysis also clarifies the role of the endpoint strategies. When stress is emphasised, raster-like behaviour becomes more favourable. When distortion is emphasised, edge-in behaviour becomes more favourable. This sensitivity indicates that single-metric ranking would be misleading. The scan-order objective in the current benchmark is better understood as a stress–distortion trade-off with competing preferences.

PEEQ contributes less to ranking separation than Mises and U3 under the current threshold. Therefore, robustness interpretation focuses primarily on the stress–distortion balance, while retaining PEEQ as part of the composite reference label vector.

Table 3: Proxy-FEA alignment summary. The table summarises v1/v2 alignment results, including the strongest target-specific proxy associations, composite-score association, pairwise agreement, and diagnostic interpretation. All entries are qualitative and exploratory due to the small  $n = 10$  evaluated set.

Version	Target	Proxy metric	Pearson	Spearman	Pairwise	Diagnostic interpretation
v1	Composite	proxy_jump_mean	-0.045	0.249	–	Weak composite-score signal; qualitative only.
v1	Mises	proxy_jump_mean	0.526	0.505	–	Moderate association, not validated as a stress proxy.
v1	U3	proxy_jump_mean	-0.842	-0.730	–	Target-specific U3/distortion-related signal.
v1	Pairwise	proxy_jump_mean	–	–	0.614	Pairwise diagnostic only; qualitative due to $n = 10$ .
v2	Composite	all_window_dispersion_mean	0.120	0.439	–	Best raw v2 composite-score signal, but not robust or actionable.
v2	Mises	early_window_pairwise_distance_mean	0.858	0.854	–	Wrong-sign diagnostic; qualitative only.
v2	U3	proxy_stress_risk_candidate	-0.622	-0.782	–	Wrong-sign diagnostic; qualitative only.
v2	Pairwise	edge_first_ratio	–	–	0.667	Slightly above v1 but still qualitative and not surrogate validation.

#### 4.5. Proxy-FEA alignment and reward mismatch

Proxy-FEA alignment results are summarised in Table 3 and Fig. 7. These results address the central RL-oriented question of whether cheap proxy metrics preserve the same preference structure as the sparse FEA reference labels, a concern closely related to reward misspecification and pairwise preference consistency in RL-oriented evaluation [19, 20]. In the current exploratory ten-strategy set, the alignment remains limited.

The v1 alignment analysis indicates that the most informative path-based proxy signal mainly captures U3- or distortion-related behaviour rather than the complete composite FEA reference score. In particular, the jump/path-spacing-related proxy metric shows stronger association with U3 distortion than with the composite reference score. This

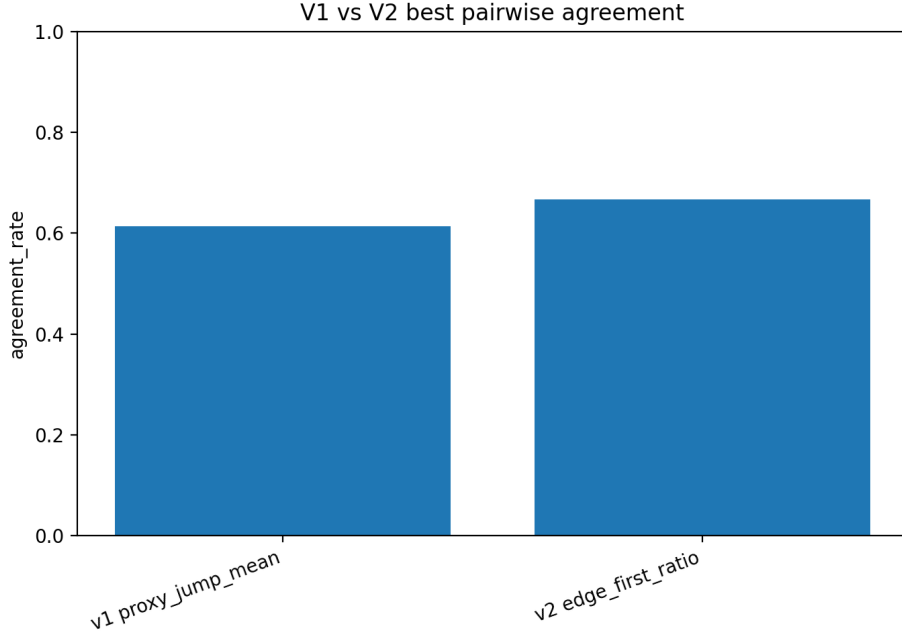


Figure 7: Proxy–FEA pairwise agreement and limitation summary. The figure compares v1 and v2 pairwise ranking agreement between proxy-induced and FEA-induced preferences. It is used to show proxy limitation and reward/world-model mismatch, not surrogate validation.

suggests that such metrics are target-specific indicators rather than complete objective predictors.

The v2 alignment analysis introduced richer sequence descriptors, including neighbour-gap, hot-cluster, boundary/symmetry, stress-risk, distortion-risk, and compromise-oriented metrics. These redesigned metrics improved some diagnostic views but did not establish a robust predictor of the sparse FEA teacher signals. In particular, the v2 compromise-oriented proxy did not identify `center_out` as the preferred compromise candidate. This is important because `center_out` is identified by the FEA reference ranking as the strongest compromise candidate within the evaluated set.

This result should be interpreted carefully. It does not mean that cheap proxy metrics are useless. The lower-level proxy remains useful for rapid candidate generation and preliminary screening. However, the present results show that the proxy cannot be treated as a stand-alone replacement for FEA reference evaluation. In RL terms, proxy-only reward design may bias future policy learning toward path-spacing or distortion-related behaviour without reliably improving the composite FEA reference objective.

Therefore, the main output of Proxy–FEA alignment is reward/world-model diagnosis.

The alignment results indicate which proxy features capture selected trends, which trends are missing, and where future reward or world-model redesign should focus. They should not be described as reward-weight calibration, surrogate validation, or proof that the cheap proxy predicts FEA outcomes.

## 5. Discussion

### 5.1. Implications for RL reward and world-model design

The results indicate that reward design for RL-guided scan-order optimisation should not rely on a single proxy objective. In the current simplified LDED32 benchmark, the FEA reference labels suggest that scan-order quality is better interpreted as a multi-metric preference problem involving residual stress, vertical distortion, and a plasticity-related indicator with limited discrimination under the selected threshold. The ranking of `center_out` as a robust compromise candidate, together with the endpoint behaviour of `raster_left_to_right` and `edge_in`, indicates that different scan orders may improve one residual outcome while worsening another. This observation highlights the importance for RL-guided scan-order optimisation, as a policy can only optimise the preference structure encoded in its reward signal. This interpretation is consistent with the broader concern that misspecified reward signals can drive learning systems toward behaviours that differ from the designer’s intended objective [19], and with the multi-objective view that competing objectives should be interpreted through trade-offs rather than a single universal optimum [21].

For future RL-guided scan-order optimisation, reward construction should therefore preserve the stress–distortion trade-off rather than collapse it prematurely into a single thermal-uniformity or path-smoothness objective. A reward term that only promotes long scan jumps, spatial separation, local cooling, or reduced reheating may be computationally attractive, but it may also emphasise only one part of the residual response. Similarly, a reward focused only on residual stress or only on distortion could drive the policy toward one endpoint of the trade-off. The present results therefore suggest that one central challenge is not only policy search, but the construction of a reward signal that reflects the relevant multi-metric preference structure.

The same implication applies to the task-level world model used to evaluate candidate scan sequences. In this paper, the world model is not a learned latent-dynamics model,

but an evaluation structure that maps scan-order decisions to approximate process-quality indicators. This distinction is important because the term world model is often associated with model-based RL and learned environment models used for planning or policy learning [17, 18]. The Proxy-FEA alignment results show that cheap path-based metrics capture selected trends, especially distortion- or spacing-related behaviour, but do not robustly preserve the sparse FEA teacher signals. This does not make proxy metrics useless; rather, it indicates that they should be treated as partial descriptors within a broader reward/world-model design.

This interpretation also clarifies the value of incomplete proxy results. The failure of the current proxy descriptors to recover the full FEA preference structure should not be viewed simply as a failed modelling attempt. Instead, it provides information about what the lower-level evaluation model is missing. For RL-guided manufacturing optimisation, such diagnostic feedback is useful because it can prevent policy learning from being driven by convenient but incomplete objectives.

### *5.2. Role of sparse FEA reference evaluation*

The results highlight the value of sparse FEA reference evaluation as a diagnostic and corrective layer for RL-oriented scan-order optimisation. Full thermo-mechanical FEA is too expensive to serve as dense feedback at every RL decision step, especially when the action sequence is long and policy training requires many rollouts. However, applying FEA sparsely to selected complete scan strategies can provide higher-cost reference information about residual outcomes that are not captured reliably by cheap proxy descriptors. This low-cost proxy plus sparse high-cost reference structure is conceptually aligned with multifidelity modelling, where inexpensive low-fidelity models are used to reduce evaluation cost while higher-fidelity evaluations remain available for correction, filtering, or optimisation support [16].

In the current workflow, the FEA reference layer serves three main functions. First, it provides a simulation-based ranking of completed scan strategies using final-cooling residual metrics. Second, it exposes the stress-distortion structure of the evaluated strategy set, including compromise and endpoint behaviours that would be difficult to infer from proxy metrics alone. Third, it enables Proxy-FEA alignment analysis, which audits whether the lower-level proxy evaluator preserves the preference structure of the FEA

reference labels. These functions make the FEA layer useful without requiring FEA to be used as a dense online reward source.

This role is especially relevant for RL because early reward design choices can strongly shape the policy search direction. If a proxy reward favours path-spacing behaviour but misses the composite stress–distortion preference, a policy trained on that proxy may converge toward a scan order that is attractive under the proxy but less favourable under the FEA reference objective. Sparse FEA reference evaluation provides a way to detect this mismatch before committing to large-scale policy training.

The FEA labels in this study should still be interpreted with care. They are simulation-based reference outcomes from a simplified whole-track heating LDED32 benchmark, not experimental ground truth. Thermo-mechanical AM simulation studies and residual-stress reviews show that residual stress and distortion are strongly dependent on modelling assumptions, process conditions, and spatial field interpretation [25, 7]. The current Abaqus model is therefore used as a reference evaluator within the diagnostic workflow, not as proof of calibrated high-fidelity LDED physics. The value of the FEA layer in this paper lies in comparative diagnosis within the current simulation setting, rather than in definitive physical validation.

### *5.3. Limitations and directions for future work*

The conclusions of this study are limited to the current simulation-based, simplified whole-track heating LDED32 stripe benchmark with ten evaluated scan strategies. The Proxy–FEA alignment results are qualitative and exploratory due to the small evaluated set. The present study does not claim final RL policy success, experimental validation, calibrated physical LDED simulation, or validated surrogate modelling. These limitations define the scope of the paper as a diagnostic benchmark and reward/world-model analysis, rather than a final demonstration of learned scan-order control.

The simplified whole-track heating abstraction is useful for examining track-order effects, but it does not resolve the full moving heat-source physics of LDED. Similarly, the fixed 32-track action space provides interpretable scan-order comparisons, but it has limited strategy entropy for strong RL policy-learning claims. Because the set of candidate strategies is compact and structured, future policies could risk learning or reproducing simple ordering patterns rather than demonstrating genuine generalisation. The cur-

rent benchmark is therefore best treated as a diagnostic benchmark closure study for reward/world-model analysis.

The next stage should increase benchmark entropy and policy-generalisation demand while retaining the bilevel Proxy–FEA logic. A natural direction is an LPBF-like two-dimensional patch or grid benchmark with variable masks, random subset targets, richer local action consequences, and multiple neighbourhood structures. Recent RL-based LPBF toolpath studies have explored adaptive scan-path generation using thermal-uniformity-oriented rewards and fast approximate thermal evaluation, illustrating the relevance of higher-entropy two-dimensional toolpath benchmarks for future policy learning [14, 15]. Such a benchmark would require policies to generalise across geometries and partial-build contexts rather than optimise a single fixed 32-track order. This would provide a more appropriate setting for evaluating whether RL can learn reusable scan-order policies.

Future proxy and world-model design should also be expanded. The current proxy descriptors mainly capture path-spacing or distortion-related trends. A richer lower-level evaluator should include local thermal-history indicators, neighbourhood exposure, path continuity, boundary effects, and candidate stress–distortion descriptors. However, these additions should not be treated as automatically validated. They should be tested through the same sparse FEA reference alignment process used here.

In this sense, the present LDED32 study closes one stage of the workflow rather than completing the full RL optimisation problem. It establishes the need for reward/world-model diagnosis, demonstrates how sparse FEA reference labels can expose proxy mismatch, and motivates a higher-entropy benchmark for future policy learning. The central continuity is not the specific 32-track geometry or the current proxy formula, but the bilevel evaluation principle: fast proxy-based candidate generation should be coupled with sparse simulation-based reference evaluation before making strong claims about RL-guided scan-order optimisation.

## 6. Conclusions

This study investigated a bilevel Proxy–FEA diagnostic approach for reinforcement-learning-guided scan-order optimisation in laser additive manufacturing. A simplified LDED32 benchmark was used to examine whether cheap scan-order proxy metrics can

provide reliable reward or world-model signals for future RL policy learning. The lower level provided fast proxy-based candidate evaluation, while the sparse Abaqus FEA reference layer supplied simulation-based residual outcome labels for selected complete scan strategies.

Within the ten evaluated scan strategies, the FEA reference results showed that scan-order performance is better interpreted as a multi-metric stress–distortion preference problem rather than a single-objective thermal-uniformity problem. `center_out` emerged as a robust compromise candidate in the evaluated set, while `raster_left_to_right` and `edge_in` represented opposing stress–distortion endpoint behaviours. The PEEQ-based plastic-fraction metric provided limited discrimination under the selected threshold.

The Proxy–FEA alignment analysis showed that the current cheap proxy descriptors capture selected trends, especially distortion- or path-spacing-related behaviour, but do not robustly recover the sparse FEA teacher signals. This indicates that proxy-only reward design may bias future RL optimisation toward incomplete objectives. Sparse FEA reference evaluation is therefore valuable as a diagnostic correction layer before large-scale policy training.

The conclusions are limited to the current simulation-based, simplified whole-track heating LDED32 benchmark. The present work does not claim final RL policy success, experimental validation, calibrated LDED physics, or a validated surrogate model. Future work should therefore move toward higher-entropy LPBF-like or patch-based benchmarks while retaining sparse FEA reference evaluation to guide reward and world-model refinement.

### **Author Contributions**

**Xian Wu:** Conceptualization, methodology, software, finite-element modelling, reinforcement-learning framework implementation, formal analysis, investigation, data curation, visualization, and writing – original draft. **Haoran Li:** Methodology, reinforcement-learning discussion, and writing – review and editing. **Dongbin Zhao:** Supervision, reinforcement-learning methodology guidance, and writing – review and editing. **Ruiyao Zhang:** Methodology, finite-element modelling guidance, additive-manufacturing process guidance, investigation, and writing – review and editing. **Yuanqi Chu:** Methodology, mathematical modelling, formal analysis, and writing – review and editing. **Bin Wang:**

Supervision, project administration, research guidance, and writing – review and editing. All authors reviewed and approved the final manuscript.

### **Declaration of Competing Interest**

The authors declare that they have no known competing financial interests or personal relationships that could have appeared to influence the work reported in this paper.

### **Acknowledgments**

The authors acknowledge Brunel University London for providing the research environment and computational/software resources that supported this work. The authors also acknowledge the use of Abaqus-based finite-element modelling and post-processing in the simulation-based reference evaluation workflow.

### **Data availability**

The data and code supporting the findings of this study are available in the project GitHub repository:

<https://github.com/BrunelXian/RL-LAM-ScanOpt>

The repository includes scripts, processed tables, figure-generation outputs, and diagnostic analysis assets used for proxy evaluation, FEA reference-label analysis, ranking robustness checks, and Proxy–FEA alignment. Large binary simulation files, including Abaqus ODB files, are not included because of file-size and software-specific storage constraints. The derived metrics and processed outputs required to reproduce the reported tables and figures are provided.

### **References**

- [1] J. Dar, A. G. Ponsot, C. J. Jolma, D. Lin, A review on scan strategies in laser-based metal additive manufacturing, *Journal of Materials Research and Technology* 36 (2025) 5425–5467. doi:10.1016/j.jmrt.2025.04.068.
- [2] W. Zhang, M. Tong, N. M. Harrison, Scanning strategies effect on temperature, residual stress and deformation by multi-laser beam powder bed fusion manufacturing, *Additive Manufacturing* 36 (2020) 101507. doi:10.1016/j.addma.2020.101507.

- [3] C.-J. Hassila, A. Malmelöv, C. Andersson, J. Hektor, M. Fisk, A. Lundbäck, U. Wiklund, Influence of scanning strategy on residual stresses in laser-based powder bed fusion manufactured alloy 718: Modeling and experiments, *Materials* 17 (24) (2024) 6265. doi:10.3390/ma17246265.
- [4] D. Xie, F. Lv, Y. Yang, L. Shen, Z. Tian, C. S. Shuai, B. Chen, J. Zhao, A review on distortion and residual stress in additive manufacturing, *Chinese Journal of Mechanical Engineering: Additive Manufacturing Frontiers* 1 (3) (2022) 100039. doi:10.1016/j.cjmeam.2022.100039.
- [5] N. Bastola, M. P. Jahan, N. Rangasamy, C. S. Rakurty, A review of the residual stress generation in metal additive manufacturing: Analysis of cause, measurement, effects, and prevention, *Micromachines* 14 (7) (2023) 1480. doi:10.3390/mi14071480.
- [6] J. Liu, J. Ye, D. Silva Izquierdo, A. Vinel, N. Shamsaei, S. Shao, A review of machine learning techniques for process and performance optimization in laser beam powder bed fusion additive manufacturing, *Journal of Intelligent Manufacturing* 34 (2023) 3249–3275. doi:10.1007/s10845-022-02012-0.
- [7] S.-H. Wu, U. Tariq, R. s. Joy, T. Sparks, A. Flood, F. Liou, Experimental, computational, and machine learning methods for prediction of residual stresses in laser additive manufacturing: A critical review, *Materials* 17 (7) (2024) 1498. doi:10.3390/ma17071498.
- [8] R. Zhang, J. Strickland, X. Hou, F. Yang, X. Li, J. A. de Oliveira, J. Li, S. Zhang, Rapid residual stress simulation and distortion mitigation in laser additive manufacturing through machine learning, *Additive Manufacturing* 102 (2025) 104721. doi:10.1016/j.addma.2025.104721.
- [9] S. Liao, S. Webster, D. Huang, R. Council, K. Ehmman, J. Cao, Simulation-guided variable laser power design for melt pool depth control in directed energy deposition, *Additive Manufacturing* 56 (2022) 102912. doi:10.1016/j.addma.2022.102912.
- [10] F. Ogoke, A. B. Farimani, Thermal control of laser powder bed fusion using deep reinforcement learning, *Additive Manufacturing* 46 (2021) 102033. doi:10.1016/j.addma.2021.102033.

- [11] S. Vagenas, G. Panoutsos, Stability in reinforcement learning process control for additive manufacturing, *IFAC-PapersOnLine* 56 (2) (2023) 4719–4724. doi:10.1016/j.ifacol.2023.10.1233.
- [12] R. d. R. Faria, B. D. O. Capron, A. R. Secchi, M. B. de Souza, Where reinforcement learning meets process control: Review and guidelines, *Processes* 10 (11) (2022) 2311. doi:10.3390/pr10112311.
- [13] C. Dou, J. Chung, R. Gnanasambandam, Y. Wu, J. Li, Z. J. Kong, Reinforced scan: a reinforcement learning enabled optimal laser scan path planning in laser powder bed fusion additive manufacturing, *The International Journal of Advanced Manufacturing Technology* 142 (9–10) (2026) 5257–5273. doi:10.1007/s00170-025-17144-9.
- [14] M. Qin, J. Ding, S. Qu, X. Song, C. C. L. Wang, W.-H. Liao, Deep reinforcement learning based toolpath generation for thermal uniformity in laser powder bed fusion process, *Additive Manufacturing* 79 (2024) 103937. doi:10.1016/j.addma.2023.103937.
- [15] T. Kim, D. Kim, S.-S. Kwon, S. L. Sing, N. Kim, I. D. Jung, Reinforcement learning-based toolpath optimisation with 3d u-net driven rapid thermal prediction, *Virtual and Physical Prototyping* 21 (1) (2026) e2627765. doi:10.1080/17452759.2026.2627765.
- [16] B. Peherstorfer, K. Willcox, M. Gunzburger, Survey of multifidelity methods in uncertainty propagation, inference, and optimization, *SIAM Review* 60 (3) (2018) 550–591. arXiv:1806.10761, doi:10.1137/16M1082469.
- [17] R. S. Sutton, Dyna, an integrated architecture for learning, planning, and reacting, *ACM SIGART Bulletin* 2 (4) (1991) 160–163. doi:10.1145/122344.122377.
- [18] D. Ha, J. Schmidhuber, World models, arXiv preprint arXiv:1803.10122 (2018). arXiv:1803.10122.
- [19] D. Amodei, C. Olah, J. Steinhardt, P. Christiano, J. Schulman, D. Mané, Concrete problems in ai safety, arXiv preprint arXiv:1606.06565 (2016). arXiv:1606.06565.

- [20] C. J. C. Burges, T. Shaked, E. Renshaw, A. Lazier, M. Deeds, N. Hamilton, G. Hultender, Learning to rank using gradient descent, in: Proceedings of the 22nd International Conference on Machine Learning, ICML '05, Association for Computing Machinery, 2005, pp. 89–96. doi:10.1145/1102351.1102363.
- [21] K. Deb, A. Pratap, S. Agarwal, T. Meyarivan, A fast and elitist multiobjective genetic algorithm: Nsga-ii, IEEE Transactions on Evolutionary Computation 6 (2) (2002) 182–197. doi:10.1109/4235.996017.
- [22] J. Goldak, A. Chakravarti, M. Bibby, A new finite element model for welding heat sources, Metallurgical Transactions B 15 (2) (1984) 299–305. doi:10.1007/BF02667333.
- [23] P. Michaleris, Modeling metal deposition in heat transfer analyses of additive manufacturing processes, Finite Elements in Analysis and Design 86 (2014) 51–60. doi:10.1016/j.finel.2014.04.003.
- [24] Q. Yang, P. Zhang, L. Cheng, Z. Min, M. Chyu, A. C. To, Finite element modeling and validation of thermomechanical behavior of ti-6al-4v in directed energy deposition additive manufacturing, Additive Manufacturing 12 (2016) 169–177. doi:10.1016/j.addma.2016.06.012.
- [25] T. Mukherjee, W. Zhang, T. DebRoy, An improved prediction of residual stresses and distortion in additive manufacturing, Computational Materials Science 126 (2017) 360–372. doi:10.1016/j.commatsci.2016.10.003.